Sea-ice growth and water-mass modification in the Mertz Glacier polynya, East Antarctica, during winter

N. L. Bindoff,[1] G. D. Williams,[1,2] I. Allison[1,3]

[1]*Antarctic CRC, University of Tasmania, Box 252-80, Hobart, Tasmania 7001, Australia*
[2]*IASOS, University of Tasmania, Box 252-77, Hobart, Tasmania 7001, Australia*
[3]*Australian Antarctic Division, Box 252-80, Hobart, Tasmania 7001, Australia*

ABSTRACT. In July–September 1999, an extensive oceanographic survey (87 conductivity-, temperature- and depth-measuring stations) was conducted in the Mertz Glacier polynya over the Adélie Depression off the Antarctic coast between 145° and 150° E. We identify and describe four key water masses in this polynya: highly modified circumpolar deep water (HMCDW), winter water (WW), ice-shelf water (ISW) and high-salinity shelf water (HSSW). Combining surface velocity data (from an acoustic Doppler current-profiler) with three hydrographic sections, we found the HMCDW to be flowing westward along the shelf break (0.7 Sv), the WW and HSSW flowing eastwards underneath Mertz Glacier (2.0 Sv) and that there was a westward return flow of ISW against the continent (1.2 Sv). Using a simple box model for the exchanges of heat and fresh water between the principal water masses, we find that the polynya was primarily a latent-heat polynya with 95% of the total heat flux caused by sea-ice formation. This heat flux results from a fresh-water-equivalent sea-ice growth rate of 4.9–7.7 cm d^{-1} and a mass exchange between HMCDW and WW of 1.45 Sv The inferred ocean heat flux is 8–14 W m^{-2} and compares well with other indirect estimates.

1. INTRODUCTION

Brine rejection during sea-ice formation plays a critical role in the increase of wintertime salinity over the continental shelf that is necessary for the formation of bottom water. Polynyas are regions where the rate of sea-ice formation may be up to 10 times greater than in the surrounding sea-ice zone (Zwally and others, 1985). A detailed census of the significant polynyas between 40° and 160° E, using satellite passive-microwave data over an 8 year period, shows that the largest and most persistent polynyas are the Shackleton Ice Shelf and the Mertz polynyas, with an average area in winter of 30 000 and 23 000 km^2, respectively (Massom and others, 1998). However, in spite of its larger size the Shackleton Ice Shelf (near 95° E) is not associated with bottom water formation (Bindoff and others, 2000a). The factors that affect ice production, and therefore brine rejection, are not limited to the size of the polynya alone, but also include the strength and direction of the local winds, and air and water temperatures. Along the Antarctic coastline, the Mertz polynya (67° S, 145° E) is in a region of some of the world's strongest and most persistent winds (Ball, 1957; Adolphs and Wendler, 1995). It is these intense meteorological conditions that give rise to the Mertz polynya having what is believed to be the greatest ice production in East Antarctica (Cavalieri and Martin, 1985).

The Mertz polynya lies immediately above the Adélie Depression (Fig. 1) and forms to the west of Mertz Glacier. Its size is also partly controlled by the line of grounded icebergs and fast ice that extends north from this glacier (at 146° E), blocking the westward flow of sea ice into the polynya area. The katabatic winds are strongly offshore at the coastline, turning westwards within 20–30 km. However,

the ice-free region extends well beyond the zone of strong winds, and this polynya (~200 km wide) is wider than most (Massom and others, 1998). Its unusual width is partly caused by the shape and northward orientation of Mertz Glacier Tongue blocking the westward transport of sea ice.
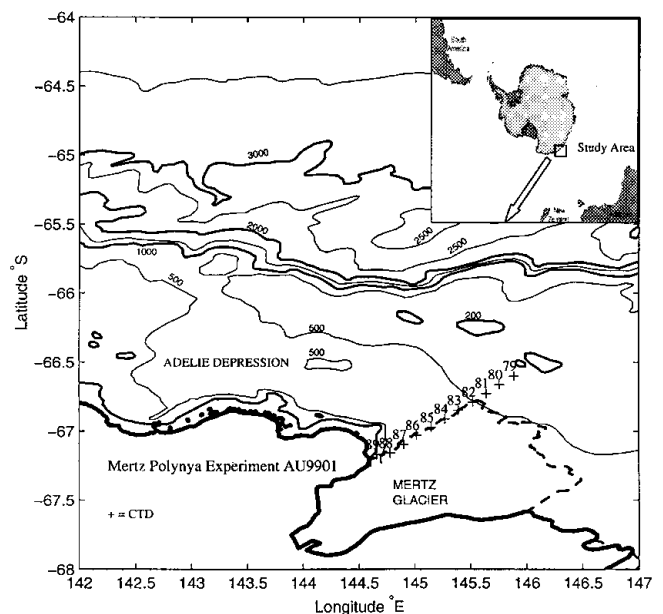

Fig. 1. The Terre Adélie coastline from 142° to 147° E, showing the geographical setting for the Mertz polynya experiment and in particular the Adélie Depression and Mertz Glacier. The locations of the CTD stations along the western edge of Mertz Glacier are shown for repeat 3 of this section (stations 79–89). (Inset: the location of Mertz polynya in Antarctica.)

However, the polynya also becomes ice-free earlier in the spring than locations immediately to the east and west (Gloersen and others, 1992; Massom and others, 1998), which may be the result of the upwelling of warm modified circumpolar deep water (MCDW) in the polynya region (Rintoul, 1998). The polynya has a strong seasonal signal, with its areal extent typically becoming largest in October, ranging from 20 000 to 60 000 km^2 (Massom and others, 1998). Its fastest rate of growth tends to occur during August–September, which is consistent with observations of maximum sea-ice production and coincides with the colder bottom waters observed in temperature time series measured offshore (Fukamachi and others, 2000).

The Australian-Antarctic basin is associated with bottom water formation off the Terre Adélie coastline near 140° E (Gordon and Tchernia, 1972). However, this source has been considered relatively weak, and the bottom waters found in this basin were thought to be the product of mixing between Ross Sea bottom water (RSBW) and Weddell Sea bottom water (WSBW) (Carmack, 1977). However, recent hydrographic observations along 140° E have shown a local maximum in bottom CFC-11 and oxygen concentrations, and a minimum in bottom temperatures (Bindoff and others, 1997; Rintoul and Bullister, 1999). This maximum in CFC-11 and oxygen concentrations cannot be obtained by mixing RSBW and WSBW in this basin, because both of these water masses have lower CFC-11 and oxygen concentrations and warmer temperatures in this basin. This suggests that the bottom waters in this basin have a local source. The identification of a source of bottom water on the continental shelf in the Adélie Depression near Mertz Glacier (Gordon and Tchernia, 1972; Rintoul, 1998) led to a reinterpretation of the volumetric census of bottom waters. This showed that Terre Adélie bottom water has a volume second only to WSBW and three times that of RSBW (Rintoul, 1998).

This paper presents the first wintertime hydrographic sections taken in this important source region of Antarctic bottom water. We describe the distribution and circulation of water masses present along three repeats of a hydrographic section across the Adélie Depression. We then develop a simple model of the major processes of interactions with the atmosphere and ice shelf operating within the Mertz polynya that are responsible for forming the observed wintertime water masses.

2. DESCRIPTION OF THE STUDY AREA

Location

Mertz Glacier exits the Terre Adélie section of the Antarctic coast at 145° E, 67° S (Fig. 1). The floating ice shelf extends over the Adélie Depression and is probably grounded on the shallow bathymetry to the north.

Over this shallow bathymetry, a line of grounded icebergs is found with the same northeast–southwest orientation as the glacier tongue. During winter, fast ice connects these icebergs to Mertz Glacier, creating a continuous zone of ice from the coast to the shelf break (Massom and others, 1998, 2001). The Mertz polynya lies immediately to the west of this barrier.

Bathymetry

The bathymetry is dominated by the Adélie Depression, a distinct basin with a maximum depth of 1200 m. A trough located at 143° E, 66° S connects the Adélie Depression across the continental shelf break to the deep ocean. The GEBCO (general bathymetric chart of the oceans) contours (Fig. 1) show that the Adélie Depression extends eastwards beneath Mertz Glacier and is closed below 500 m. However, other maps east of Mertz Glacier show a trough deeper than 500 m connecting the depression to the shelf break (Rintoul, 1998).

The observation program

Between 29 July and 23 August 1999, 87 conductivity-, temperature- and depth-measuring (CTD) stations were occupied within the Adélie Depression as part of a joint sea-ice oceanography project investigating the Mertz polynya in austral winter. Three occupations of a closed loop against the Antarctic coastline and along Mertz Glacier were undertaken (74 stations). The loop was positioned to enclose the central area of the polynya and trace the edge of Mertz Glacier along its western flank. A number of other stations were occupied in the western trough between the depression and the shelf break, and along the shelf break towards Mertz Glacier.

Vertical profiles of conductivity, temperature and pressure were obtained with a Neil Brown Mk 3 (World Ocean Circulation Experiment (WOCE) upgrade) CTD device. Each cast was to within 10 m of the bottom. On each CTD cast, water samples were taken at selected depths with Niskin bottles deployed on a 12-bottle rosette. The calibrated CTD salinity data were analyzed with a rms precision of 0.003 psu (practical salinity units) and an overall accuracy of 0.002 psu. Temperature and pressure calibrations of the CTD before and after the cruise produced an accuracy of the CTD temperature and pressure data of 0.001 °C and 6 dbar, respectively. Niskin bottle samples were also analyzed for dissolved oxygen concentrations using standard WOCE methods and are accurate to 1% (Saunders, 1991). The primary focus is on the three eastern sections of each loop along the edge of Mertz Glacier Tongue (repeat 1: stations 22–31; repeat 2: stations 46–56; repeat 3: stations 79–89) (see Fig. 1). The nominal station spacing along the Mertz section was 5 nautical miles.

Data were also collected from an acoustic Doppler current-profiler (ADCP) mounted in the hull of the RSV *Aurora Australis* behind an 81 mm polyethylene window. Orientation and speed of the ship was provided by an Ashtech three-dimensional global positioning system. These data were calibrated for bias and misalignment errors using both bottom tracking and acceleration methods. However, certain systematic biases occur when the ship is underway. In this paper we use only the best-quality ADCP data, collected when the RSV *Aurora Australis* was either on station or moving at a speed of < 0.35 m s^{-1}.

3. PROPERTY DISTRIBUTIONS AND CIRCULATION

The temperature and salinity section along Mertz Glacier from the third and first repeats of the section (Figs 2 and 3, respectively) shows four distinct water masses and two frontal systems. This section was collected towards the end of the voyage (19–21 August) after an intense outbreak of cold air temperatures off the continent. The warmest waters (> −1.88°C) are observed on the northern side of the Adélie Depression, and the coldest at the southern end (< −2.0°C). The coldest waters form a local minimum at 300 dbar adjacent to the continent.
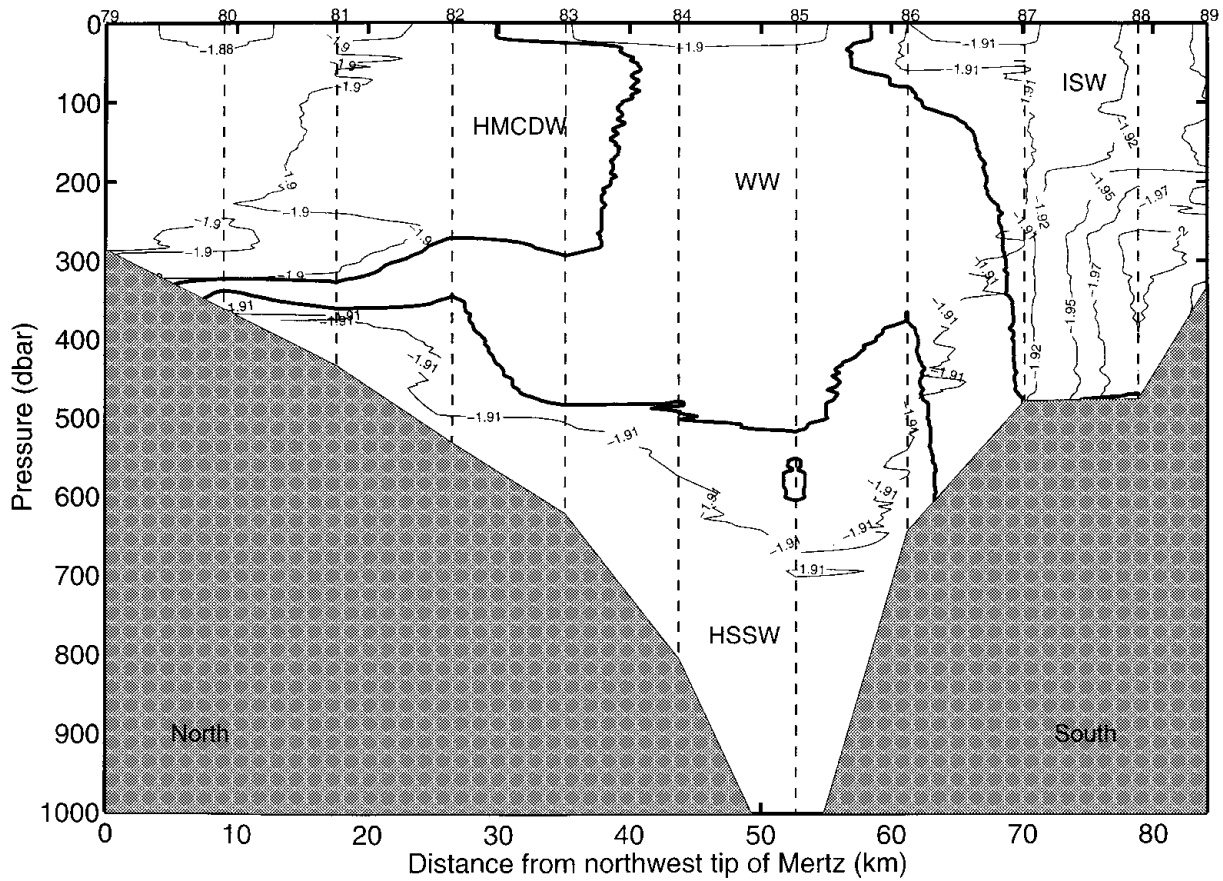
Fig. 2. The potential temperature field (°C) along the section taken on repeat 3. CTD station numbers are shown along the top, the x axis representing the distance along Mertz Glacier from the northwest tip (top right corner) to the Antarctic coast. Isotherms are contoured from average 2 dbar CTD data, and the bottom topography from maximum pressures recorded by the CTD. Isotherms are the thin lines, and the thick lines are the isopycnals separating the water masses shown in Table 1.
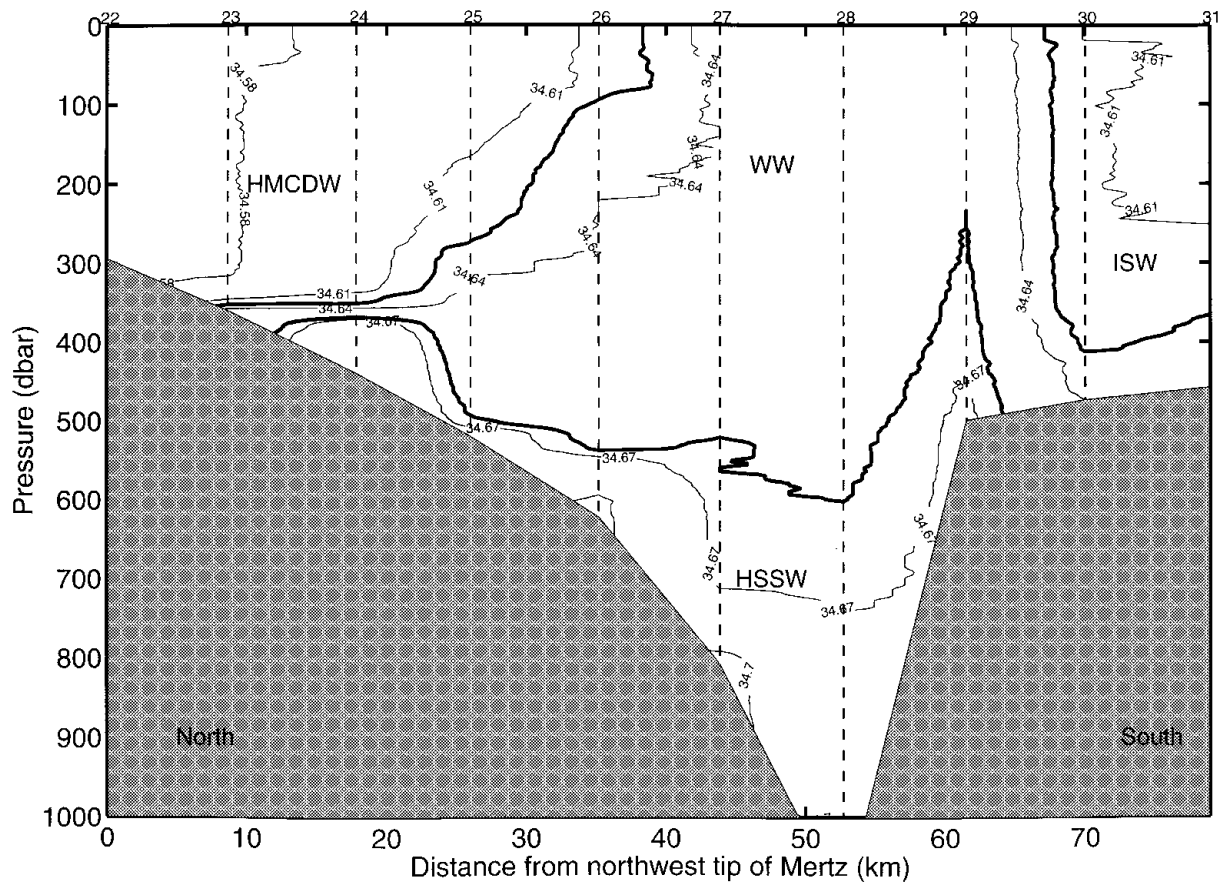

Fig. 3. The salinity field (psu) along the section taken on repeat 1 (stations 22–31). The station locations are the same as those for repeat 3 shown in Figure 1.

	Potential density	Area-averaged salinity	Area-averaged potential temperature
	kg m^3	psu	°C
HMCDW	<27.88	34.586	−1.898
WW	27.88–27.91	34.644	−1.907
ISW	<27.88	34.602	−1.931
HSSW	>27.91	34.680	−1.910

While the temperature section along Mertz Glacier is relatively simple, the salinity section is more complex. This is best seen in repeat 1 (Fig. 3), where the freshest waters occur near the surface to the north and progressively increase in salinity through a front into a region of very uniform salinity that extends from near the surface to 300–400 dbar. Further south, there is another strong gradient in salinity, with the fresher values observed close to the continent. The most saline waters in this experiment (>34.7 psu), were found below a relatively homogeneous layer located over the middle of the depression and its northern flank.

In the salinity section, two fronts were observed. The first occurs on the northern side of the depression between stations 26 and 27. On the southern side of the depression there is a second front between stations 29 and 30. All three repeats of this section showed these two fronts. Although their position varied on each occasion, they are typified by a single potential density contour (Table 1). Both the northern and southern fronts are associated with a 27.88 kg m^{-3} potential density surface (Figs 2 and 3, shown as thick contours). The thick, relatively homogeneous water that lies between these two fronts is bounded at depth by the 27.91 kg m^{-3} potential density surface.

These horizontal gradients in the salinity (and hence density field) imply significant vertical shear in the ocean currents through this section. However, because of the difficulty in determining the precise reference velocity to use with the density field alone, we have used the horizontal components of the surface velocities from the ADCP measurements rotated normal to the section. The ADCP coverage along the section is not always complete, so the ADCP reference velocity field has been averaged over all three repeats of this section. This averaged reference velocity has been added to the geostrophic velocity field obtained by integrating the thermal wind equations from the surface to the ocean floor. In this way, the horizontal velocity through each vertical section was formed (third repeat is shown in Fig. 4). The maximum rms variability of the averaged ADCP velocities of about 9 cm s^{-1} is an estimate of the uncertainty in the surface reference velocity (and velocity field at depth).

The ADCP surface reference (at 20 dbar) is quite large compared to the contribution to the velocity from the thermal wind equations and makes the velocity field largely barotropic. In the following, the flow is examined in terms of the velocity component normal to the section. Although
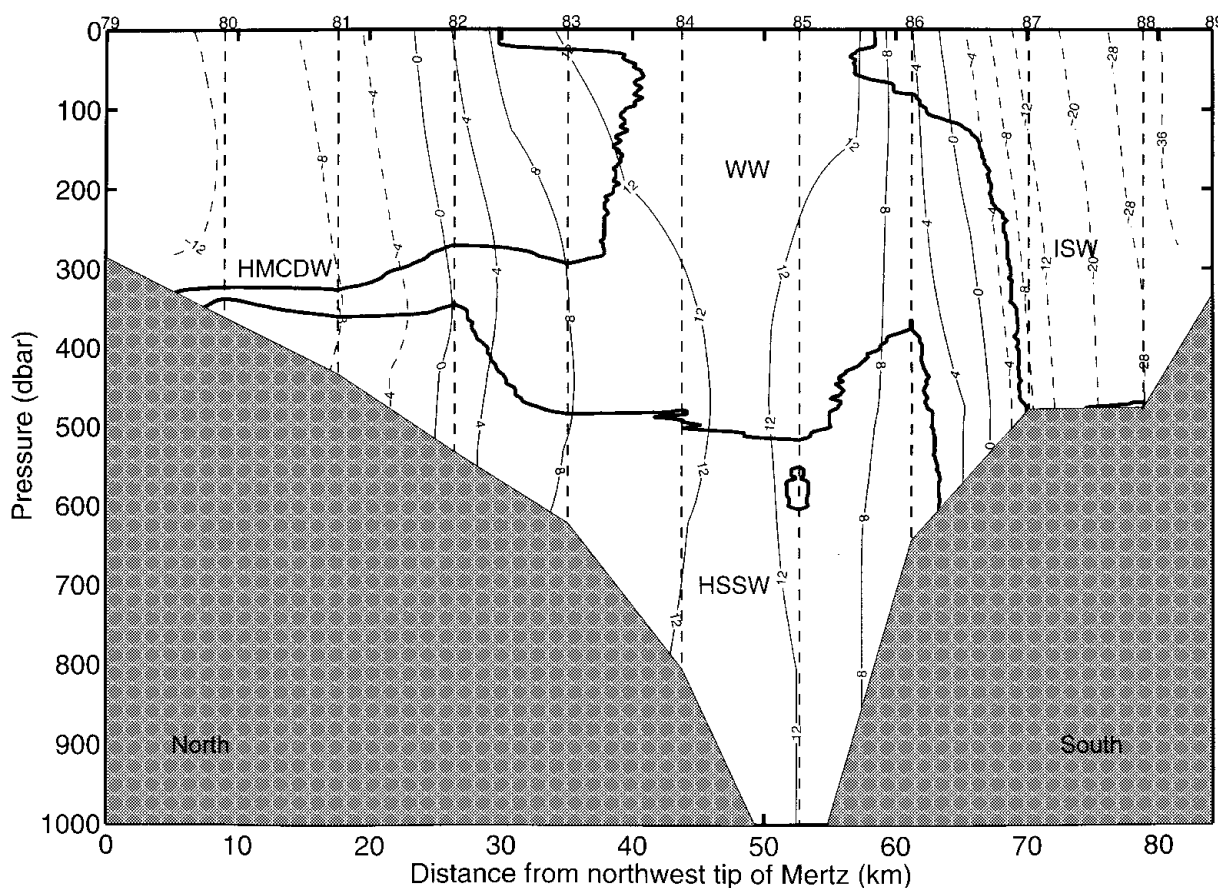

Fig. 4. *The geostrophic velocity field (cm s^{-1}) normal to the section along Mertz Glacier for repeat 3, referenced to the average surface ADCP velocities.*
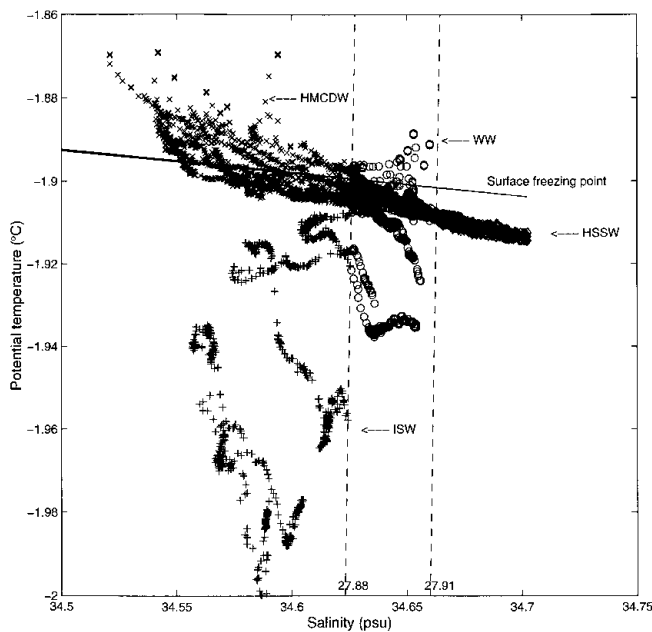
Fig. 5. *θ–S scatter plot of all 2 dbar CTD data collected along the section (stations 22–31, 46–56, 79–92). Lines of constant σ_θ are superimposed (dashed line) to highlight water-mass boundaries defined in Table 1. Shown also is the surface freezing-point curve (continuous line).*

Fig. 6. *O_2–S scatter plots of all CTD bottle data collected on all three sections (stations 22–31, 46–56, 79–92).*

the section does not run north–south, the direction of this component will subsequently be expressed as either eastward or westward. On the northern side of the Adélie Depression in ocean depths shallower than 500 dbar the flow field is westward (out of page). Over the Adélie Depression in ocean depths of >500 dbar the direction of the flow field changes to eastward, i.e. into Mertz Glacier, before returning westward again in the shallower waters near the Antarctic continent. This westward return flow adjacent to Antarctica is where the flow is strongest, exceeding 20 cm s^{-1}, and is quite narrow compared to the currents to the north.

4. WATER MASSES

We identify four distinct water masses in the CTD data in this section. The relatively warm, fresh and oxygen-poor water found north of the northern front is termed highly modified circumpolar deep water (HMCDW) (Figs 5 and 6). The relatively homogeneous and non-stratified water between the two fronts is called winter water (WW), and the cold water south of the southern front is called ice-shelf water (ISW). The densest water that lies in the Adélie Depression is typically deeper than 500 dbar and bounded above by a 29.1 kg m^{-3} potential density surface, and is termed high-salinity shelf water (HSSW). The bounding properties for each of these four water masses are listed in Table 1 and are marked in Figures 2–4.

These definitions differ from those of Rintoul (1998) and Whitworth and others (1998), but are consistent with the frontal locations and boundaries of the water masses observed in winter. HMCDW is equivalent to the densest varieties of MCDW presented in the nomenclature of Whitworth and others (1998). Our WW and HSSW are both dense enough to be classified as shelf water in their scheme. The key distinction between our WW and HSSW is that WW is weakly
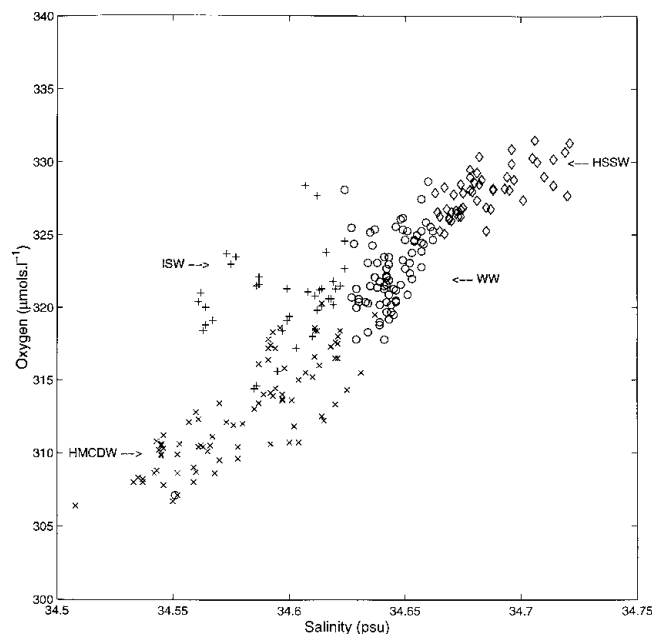
stratified while HSSW is more strongly stratified and much saltier (>34.66 psu).

The potential temperature and salinity diagram shows a strong relationship between HMCDW, WW and HSSW (Fig. 5). HMCDW, WW and HSSW have a broadly linear relation between the coldest and saltiest forms of HSSW and the warmest and freshest forms of HMCDW. The HSSW shows the least scatter from this linear relation, consistent with the water mass being isolated from the atmosphere (at the time of collection). Although the HSSW is colder than the surface freezing point, it is not supercooled compared with the freezing temperature at 40 dbar, suggesting that it was formed near the surface (unlike ISW). The WW (27.91–27.88 kg m^{-3} potential density) shows much more scatter from this linear relationship, being both warmer and cooler. The warm varieties of the WW occurred in repeat 2 when temperatures in the region were relatively high, and the cold forms of WW are actually slightly supercooled, reflecting contact with Mertz Glacier. It is likely that this variability in the WW properties and its low stratification reflects the interaction of this water mass with the atmosphere or ice shelf. The fourth water mass, ISW, is very distinctive as a result of being much colder (<−2.0°C) than the other three water masses. This water is sufficiently cold to have originated from beneath Mertz Glacier. ISW does not belong to the linear relation between HSSW and HMCDW, and its properties are a result of its contact with Mertz Glacier.

A similar linear relation can be clearly seen in the oxygen concentration and salinity diagram (Fig. 6). HMCDW has the lowest concentrations of oxygen. Through the ocean–atmosphere interaction of the polynya processes, the oxygen concentration increases linearly through the conversion of the HMCDW (~82% saturation) into WW and HSSW (~88% saturation). Although the HSSW is cut off from the atmosphere, it is higher in both salinity and oxygen, suggesting that it could have formed earlier in the winter prior to these measurements. As found in *T–S* space, the oxygen concentration of the ISW places it off the linear relation

403

Table 2. Cross-sectional area averaged properties for the water masses designated in Table 1 along the section shown in Figure 1

	Area-averaged parameters	Repeat 1	Repeat 2	Repeat 3
HMCDW	Area (m^2)	1.047×10^7	1.653×10^7	9.607×10^6
	Salinity (psu)	34.5911	34.5820	34.5837
	Pot. temperature (°C)	-1.9007	-1.8947	-1.8987
	Oxygen (μmol L^{-1})	313.7	312.2	313.5
	Velocity (cm s^{-1})	-6.880	-1.148	-3.979
	Transport (m^3 s^{-1})	-7.203×10^5	-1.898×10^5	-3.822×10^5
WW	Area (m^2)	2.202×10^7	1.922×10^7	1.740×10^7
	Salinity (psu)	34.6446	34.6435	34.6426
	Pot. temperature (°C)	-1.9060	-1.9087	-1.9057
	Oxygen (μmol L^{-1})	323.5	321.2	322.5
	Velocity (cm s^{-1})	6.619	2.312	7.631
	Transport (m^3 s^{-1})	1.458×10^6	4.446×10^5	1.328×10^6
ISW	Area (m^2)	3.520×10^6	4.735×10^6	7.658×10^6
	Salinity (psu)	34.6113	34.5977	34.5967
	Pot. temperature (°C)	-1.9123	-1.9392	-1.9404
	Oxygen (μmol L^{-1})	321.7	319.4	321.3
	Velocity (cm s^{-1})	-21.549	-23.515	-22.078
	Transport (m^3 s^{-1})	-7.585×10^5	-1.113×10^6	-1.691×10^6
HSSW	Area (m^2)	9.705×10^6	9.599×10^6	1.222×10^7
	Salinity (psu)	34.6753	34.6757	34.6796
	Pot. temperature (°C)	-1.910	-1.911	-1.911
	Oxygen (μmol L^{-1})	329.2	327.3	327.9
	Velocity (cm s^{-1})	8.598	9.063	8.845
	Transport (m^3 s^{-1})	8.345×10^5	8.699×10^5	1.082×10^6
	Total transport (m^3 s^{-1})	8.132×10^5	1.132×10^4	3.370×10^5

Notes: Potential temperatures are referenced to the surface. Velocities are the component normal to the section. The geostrophic velocities are referenced to the surface ADCP velocities averaged over all three sections. Negative velocity and transports indicate westward flow. (Repeat 1: stations 22–31; repeat 2: stations 46–56; repeat 3: stations 79–89.)

between HMCDW and HSSW. Note also that the oxygen concentration of ISW is slightly less than that in WW and significantly less than that in HSSW. Interestingly, all four water masses are well beneath the oxygen saturation limit of approximately 380 μmol kg^{-1} prescribed by the temperature range of the samples.

5. DISCUSSION

The area-averaged properties of cross-sectional area, salinity, temperature, oxygen concentration, velocity and mass transport (normal to the section along Mertz Glacier) are presented for the individual water masses, in each section, in Table 2. The distribution of these water masses and their variability and transport through the sections suggests an overall pattern of circulation. The HMCDW is moving westwards along the shelf break north of the polynya with a transport of 0.7 Sv. The linear relation on the temperature–salinity diagram suggests that the WW waters are derived from the HMCDW. This transformation occurs through the direct interaction of the HMCDW with the cold atmosphere in the polynya region. The loss of heat and brine rejection from the formation of sea ice causes vertical convection within the WW layer, leading to a relatively salty and vertically homogeneous water mass. WW has the greatest cross-sectional area, of $\sim 2 \times 10^7$ m^2, and is about twice the area of HMCDW, four times the area of ISW and twice the area of HSSW. Both WW and HSSW flow eastwards through the
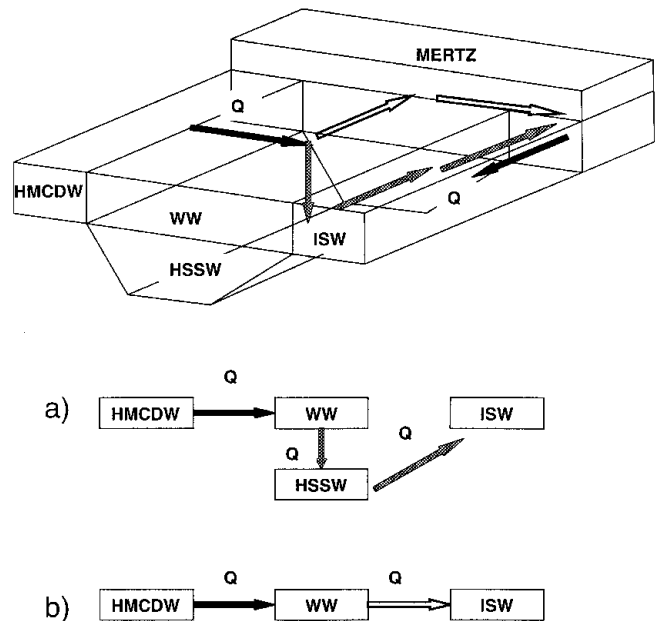

Fig. 7. Model of the exchange between HMCDW, WW, HSSW and ISW used to estimate heat and fresh-water transports. (a) Scenario prior to the voyage where WW exchanges with HSSW which then exchanges with ISW. (b) Scenario during voyage where WW exchanges directly with ISW.

section, with a transport of 1.1 and 0.9 Sv, respectively, for a total of 2 Sv. These waters are modified by their interaction with Mertz Glacier and cooled and freshened to form ISW. About 60% of these two eastward-flowing water masses return as the fast narrow ISW current of 1.2 Sv against the Antarctic continent (Fig. 4).

Using this circulation pattern, a simple model (Fig. 7) was developed for estimating the ice production and heat flux of the entire polynya/glacier system for which we chose two distinct flow patterns. The first is associated with the observations taken during the experiment, where HMCDW is converted initially into WW and then into ISW (Fig. 7b). The pycnocline separating WW from the underlying HSSW (Fig. 3) suggests that these water masses were not actively mixing together during the experiment, and the reduction in cross-sectional area of WW by 50% during the experiment supports this idea (Table 2). The second flow pattern is associated with a time period prior to the voyage (Fig. 7a) where there is active formation of HSSW and it interacts with Mertz Glacier to form ISW. This flow pattern represents the process that would create the greatest brine rejection from sea-ice formation.

Although the volume transports through the section for each of the water masses shown in Table 2 vary significantly (0.2–1.5 Sv), we have assumed that the volume exchange (Q_{mass}) between all water masses and for both flow patterns is constant. The flux of heat (Q_{heat}) and freshwater ($Q_{freshwater}$) through the surface area of the polynya (A_p) between two water masses can then be calculated as,

$$Q_{heat} = \frac{C_p \rho (\theta_2 - \theta_1) Q_{mass}}{A_p} \qquad (1)$$

$$Q_{freshwater} = \frac{(S_2 - S_1) Q_{mass}}{S_0 A_p}, \qquad (2)$$

where θ and S are the observed area-averaged potential temperature and salinity values for each water mass. The sub-

Table 3. Fresh-water and heat exchanges using Equations (1) and (2) for the area-averaged water-mass properties sampled from repeat 1 (Table 2)

Process	Ice growth/ melt rate	Latent heat	Sensible heat	Total heat transfer	Flushing rate
	cm d^{-1}	W m^{-2}	W m^{-2}	W m^{-2}	days
Before AU9901					
HMCDW to WW	−4.9	188.7	7.7	196.3	32
WW to HSSW	−2.8	108.2	6.1	114.4	15
HSSW to ISW	5.8	−225.6	3.0	−222.6	6
Total	−1.9	71.3	16.8	88.1	
During AU9901					
HMCDW to WW	−4.9	188.7	7.7	196.3	32
WW to ISW	3.0	−117.4	9.1	−108.3	6
Total	−1.9	71.3	16.8	88.1	

scripts indicate the different water masses. The S_0 term in Equation (2) is the average salinity between the two water masses for which the fresh-water exchange is being calculated. These equations are a simplification of the equations used to calculate heat and fresh-water transports beneath the Amery Ice Shelf by Wong and others (1998). The greatest mass transport, found for WW, is 1.458 Sv eastwards, with the other water masses approximately half this value. The total transport across the section was calculated and indicates that for each repeat there is a mass imbalance into the section of 0.01–0.81 Sv.

The size of the Mertz polynya has been estimated using passive-microwave data as ∼20 000 km^2 (Massom and others, 1998). This area, approximately defined by the 100 km length of the glacier and a width 200 km to the west, is much larger than the actual open-water area available to interact directly with the atmosphere during the experiment (Massom and others, 2001, fig. 1 and table 1). Here we choose the effective open-water area, A_p, to be 20% of the reported area, or 4000 km^2, to represent the total open-water component fraction of the polynya. This open area represents an average ice concentration of 80% and can be quite variable in space and season. The results presented in Table 3 are sensitive to this estimate of open area. A mass exchange (Q_{mass}) of 1.45 Sv between water masses was chosen. These two choices are somewhat arbitrary, but are consistent with the mass transport of WW and the mass exchange required to give the observed sea-ice growth in the polynya region (Lytle and others, 2001).

Using these parameters, and Equations (1) and (2), the "during-voyage" ice-production rate and heat flux out of the polynya are estimated to be 4.9 cm d^{-1} and 196.3 W m^{-2}, respectively. In the scenario suggested for the period prior to the voyage, when the polynya processes were strong enough to produce HSSW, the corresponding results were 7.7 cm d^{-1} and 310.7 W m^{-2}. Sea-ice production rates estimated from direct observations of the sea-ice conditions during the voyage are approximately 7 cm d^{-1}, and in more extreme conditions could reach 10 cm d^{-1} (Lytle and others, 2001). Because of the high salinity of the sea ice (∼10 psu), 7 cm d^{-1} represents ∼5 cm d^{-1} of fresh water.

The total heat exchange includes the sensible-heat contribution from advection between the water masses and the latent heat associated with the formation of sea ice. The

sensible-heat contribution in converting HMCDW to WW is about 7.7 W m^{-2} and represents only 3.9% of the total heat budget required for this conversion of 196.3 W m^{-2} (Table 3). Similarly, for the conversion of WW to HSSW in the "before-voyage" scenario, the sensible heat is just 6.1 W m^{-2} and represents 5.3% of the total heat budget. This low contribution occurs because the HMCDW is almost at freezing temperature and thus there is little scope for heat exchange between HMCDW and WW (or HSSW) through advection. By comparison, the salinity differences between HMCDW and WW or HSSW are large, and in terms of brine rejection imply large heat losses to the atmosphere from the ocean through sea-ice formation.

Although the ocean heat fluxes are small (13.8 W m^{-2} for HMCDW to HSSW and 7.7 W m^{-2} for HMCDW to WW) compared to the latent-heat fluxes, they are in good qualitative agreement with other direct and indirect measures of ocean heat fluxes. Lytle and others (2000) estimate ocean heat fluxes of 13.0–14.5 W m^{-2} over the Antarctic Divergence at 140° E. In the Weddell Gyre, Fahrbach and others (1994) estimate 19 W m^{-2}, while from observations of fast ice, Heil and others (1996) found a heat-flux range of 0–18 W m^{-2}. Similarly, the estimates of ocean heat fluxes inferred from models are 5–30 W m^{-2} depending on the season (Wu and others, 1997).

The production of ISW is normalized to the area of the polynya for comparison with the sea-ice production rate. We find that in terms of the complete Mertz polynya/glacier system, the contribution of fresh water and heat loss from the base of the glacier are respectively 3.0 cm d^{-1} and 108.3 W m^{-2} during the voyage and 5.8 cm d^{-1} and 222.6 W m^{-2} at the time of HSSW formation.

The net fresh-water input from the Mertz polynya/glacier system is the sum of the contributions from the ice production in the polynya and meltwater from the glacier. In the case of the before-voyage and during-voyage flow patterns, the meltwater from Mertz Glacier compensates 75% and 61% of the brine production from sea-ice formation, respectively. In both scenarios the sea-ice production is greater than the input of glacier meltwater, but close enough to suggest that during summer the region may be a net exporter of fresh water.

However, we found that of the four water masses reported here, ISW experienced the greatest change in cross-sectional area-averaged salinity and temperature over the period of the experiment, becoming steadily fresher (34.61–34.59) and significantly colder (−1.91° to −1.94°C). This result could be explained by the recirculation of waters beneath the glacier, increasing the loss of heat and injection of fresh water, but implies that the greatest uncertainty in our estimates of the net fresh-water flux is the meltwater contribution from Mertz Glacier. Our estimate of this contribution (for the conversion of WW to ISW), 44 Gt a^{-1}, is more than twice the melt rate estimated for Amery Ice Shelf, 10–21.9 Gt a^{-1} (Wong and others, 1998).

The estimated flushing times of each of the water masses give an indication of how quickly each water mass could be overturned. WW has the largest cross-sectional area (and therefore volume), and subsequently has the longest flushing time of 32 days, while ISW has the shortest flushing time of 6 days. These time-scales are short enough for the seasonal cycle to control the wintertime water-mass distributions over the shelf and are consistent with the absence of WW during summer.

6. CONCLUSIONS

The calculations of ice production (4.9–7.7 cm d^{-1} fresh-water equivalent) and corresponding heat transfer (196–310 W m^{-2}) from the Mertz polynya, using fresh-water and heat-transport analysis of the water-mass properties sampled along the western edge of Mertz Glacier, are consistent with sea-ice observations. The WW and HSSW constitute most of the water found in the depression and are found to have an easterly flow. This flow is in almost the opposite direction to the drifting buoys deployed in the same area (Lytle and others, 2001) and suggests that locally the circulation of WW is controlled by pressure gradients within the water column rather than by the local winds.

A number of questions arise from this study regarding the mechanism of bottom water formation from the Mertz polynya area. The salinity of the WW is sufficiently high to become bottom water (Bindoff and others, 2000b). Unlike HSSW, this water is not trapped by the Adélie Depression, but it is possible that the volume of HSSW does increase sufficiently to spill out of the trough and down the continental slope. The question of how and when HSSW is formed is also important. Although the RSV *Aurora Australis* was in the polynya for 1 month during winter, none of the CTDs revealed convection through the entire water column in the depression. This suggests that HSSW was formed either earlier in the season, or over shallow topography (<100 dbar) and then drained into the depression.

ACKNOWLEDGEMENTS

REFERENCES

Adolphs, U. and G. Wendler. 1995. A pilot study on the interactions between katabatic winds and polynyas at the Adélie Coast, eastern Antarctica. *Antarct. Sci.*, **7**(3), 307–314.

Ball, F. K. 1957. The katabatic winds of Adélie Land and King George V Land. *Tellus*, **9**(2), 201–208.

Bindoff, N. L., M. J. Warner and S. Nicol. 1997. The Antarctic Margin Experiment. *International WOCE Newsletter*, **26**, 36–38.

Bindoff, N. L., M. A. Rosenberg and M. J. Warner. 2000a. On the circulation and water-masses over the Antarctic continental slope and rise between 80 and 150°E. *Deep-Sea Res., Ser. II*, **47**(12–13), 2299–2326.

Bindoff, N. L., S. R. Rintoul and R. Massom. 2000b. Polynya and bottom water formation south of Tasmania. *Pap. Proc. R. Soc. Tasmania*, **133**(3), 51–56.

Carmack, E. C. 1977. Water characteristics of the Southern Ocean south of the Polar Front. *In* Angel, M., *ed. Voyage of discovery. George Deacon 70th anniversary volume.* Oxford, Pergamon Press, 15–41.

Cavalieri, D. J. and S. Martin. 1985. A passive microwave study of polynyas along the Antarctic Wilkes Land coast. *In* Jacobs, S. S., *ed. Oceanology of the Antarctic continental shelf.* Washington, DC, American Geophysical Union, 227–252. (Antarctic Research Series 43.)

Fahrbach, E., G. Rohardt, M. Schröder and V. Strass. 1994. Transport and structure of the Weddell Gyre. *Annales Geophysicae*, **12**(9), 840–855.

Fukumachi, K. and others. 2000. Seasonal variability of bottom water properties off Adélie Land, Antarctica. *J. Geophys. Res.*, **105**, 6531–6534.

Gloersen, P., W. J. Campbell, D. J. Cavalieri, J. C. Comiso, C. L. Parkinson and H. J. Zwally. 1992. *Arctic and Antarctic sea ice, 1978–1987: satellite passive-microwave observations and analysis.* Washington, DC, National Aeronautics and Space Administration. (NASA SP-511.)

Gordon, A. L. and P. Tchernia. 1972. Waters of the continental margin off Adélie coast, Antarctica. *In* Hayes, D. E., *ed. Antarctic oceanology II: the Australian–New Zealand sector.* Washington, DC, American Geophysical Union, 59–69. (Antarctic Research Series 19.)

Heil, P., I. Allison and V. I. Lytle. 1996. Seasonal and interannual variations of the oceanic heat flux under a landfast Antarctic sea ice cover. *J. Geophys. Res.*, **101**(C11), 25,741–25,752.

Lytle, V. I. and 6 others. 2001. Ice formation in the Mertz Glacier polynya, East Antarctica, during winter. *Ann. Glaciol.*, **33** (see paper in this volume).

Lytle, V. I., R. Massom, N. Bindoff, A. Worby and I. Allison. 2000. The Winter-time heat flux to the underside of east Antarctic pack ice. *J. Geophys. Res.*, **105**(C12), 28,759–28,769.

Massom, R. A., P. T. Harris, K. J. Michael and M. J. Potter. 1998. The distribution and formative processes of latent-heat polynyas in East Antarctica. *Ann. Glaciol.*, **27**, 420–426.

Massom, R. A., K. L. Hill, V. I. Lytle, A. P. Worby, M. Paget and I. Allison. 2001. Effects of regional fast-ice and iceberg distributions on the behaviour of the Mertz Glacier polynya, East Antarctica. *Ann. Glaciol.*, **33** (see paper in this volume).

Rintoul, S. R. 1998. On the origin and influence of Adélie Land bottom water. *In* Jacobs, S. S. and R. F. Weiss, *eds. Ocean, ice and atmosphere: interactions at the Antarctic continental margin.* Washington, DC, American Geophysical Union, 151–172. (Antarctic Research Series 75.)

Rintoul, S. R. and J. L. Bullister. 1999. A late winter hydrographic section from Tasmania to Antarctica. *Deep-Sea Res., Ser. I*, **46**, 1417–1454.

Saunders, P. M. 1991. Calibration and standards. *In* Joyce, T., *ed. WOCE operations manual.* Woods Hole, MA, WHP Office, 1–11.

Whitworth, T., III, A. H. Orsi, S.-J. Kim and W. D. Nowlin, Jr. 1998. Water masses and mixing near the Antarctic Slope front. *In* Jacobs, S. S. and R. F. Weiss, *eds. Ocean, ice and atmosphere: interactions at the Antarctic continental margin.* Washington, DC, American Geophysical Union, 1–27. (Antarctic Research Series 75.)

Wong, A. P. S., N. L. Bindoff and A. Forbes. 1998. On bottom water formation and ocean–ice shelf interaction in Prydz Bay, Antarctica. *In* Jacobs, S. S. and R. F. Weiss, *eds. Ocean, ice and atmosphere: interactions at the Antarctic continental margin.* Washington, DC, American Geophysical Union, 173–187. (Antarctic Research Series 75.)

Wu, X., I. Simmonds and W. F. Budd. 1997. Modeling of Antarctic sea ice in a general circulation model. *J. Climate*, **10**(4), 593–609.

Zwally, H. J., J. C. Comiso and A. L. Gordon. 1985. Antarctic offshore leads and polynyas and oceanographic effects. *In* Jacobs, S. S., *ed. Oceanology of the Antarctic continental shelf.* Washington, DC, American Geophysical Union, 203–226. (Antarctic Research Series 43.)